POWDERMET2019 Phoenix
AM2PM 2019 Additive Manufacturing With Powder Metallurgy

HOWARD I. SANDEROW OUTSTANDING TECHNICAL PAPER

THE SUPPORT EFFECT AND ITS IMPACT ON THE DESIGN OF COMPLEX-SHAPED SINTERED PM PARTS

Markus Schneider* and Virgiliu A. Savu**

Sintered powder metallurgy (PM) parts are considered to be lower in strength due to their inherent porosity and their resulting reduced load-bearing cross-section. This assumption holds true for smooth, unnotched components. However, real components used in automotive, industrial, and aerospace applications exhibit functional geometrical elements, e.g., holes, shoulder fillets, teeth, protuberances, changing cross-sections, and keyways. Therefore, smooth, unnotched components are not of practical interest. Sintered PM parts have been known to be less notch-sensitive for a long time. This behavior is of special interest because it perfectly matches the resulting stress concentrations due to the functional geometrical elements mentioned. This paper presents the results obtained from a large number of fatigue experiments. Moreover, the low notch-sensitivity of sintered PM steels is explained as a superposition of local yielding, decelerated crack growth, and statistical considerations. A correction factor, referred as the "support factor," is derived to correct linear-elastic stress results from FEA calculations to approximate the real behavior of sintered PM steels. The support effect of sintered PM steels is compared with recommendations from the German FKM (Festigkeitsnachweis für Maschinenbauteile) guideline.

INTRODUCTION

Stress concentrations ("stress raisers") are critical hot spots in the fatigue design of cyclically loaded parts. Therefore, designers have to reduce the stress-concentration effect by optimization of the part geometry. (Application of the Baud curve, Mattheck's tensile triangles, or other splines). If geometric optimization is not possible, a material class with a lower notch-sensitivity must be chosen. This is the common case for the powder metallurgy (PM) community. This paper describes a method to analyze and to implement the notch sensitivity of sintered PM steels into the FEA simulation-based fatigue assessment. The material-class dependent notch-sensitivity has been investigated for decades for gray cast iron variants. Therefore, a brief comparison between these two material classes is presented to point out some valid and some invalid similarities and to facilitate the reader's understanding. The theory and the consequences of the support effect are discussed briefly. Moreover, the theoretical predictions are compared with a huge in-house data pool. From that comparison it is evident that sintered PM steels have a strong advantage. But that advantage must be communicated in a proper way to the customer and to their modeling and simulation departments. Otherwise the strong support effect will be neglected; possibly leading to a no-go decision for sintered PM steels.

SIMILARITIES BETWEEN SINTERED PM STEELS AND GRAY CAST IRON

There are some similarities between sintered PM steels and gray cast iron variants. These similarities are helpful since the casting community is much larger than the PM community. Therefore, the PM community can adopt some findings such as those compiled in Table I to save some experiments and to minimize the testing effort. However, the correct adoption of the similarities must be proven and the supporting physics must be carefully examined. A few similarities given in Table I will be discussed very briefly. The pores reduce the stiffness of PM steels just as the lamellar graphite flakes reduce the stiffness of gray cast iron variants. Trapped gas in PM steels and the lamellar graphite flakes in gray cast iron variants affect the load-bearing cross-section. Since their contribution to the global material stiffness is negligible, the resulting

Presented at POWDERMET2019 and published in Advances in Powder Metallurgy & Particulate Materials—2019, proceedings of the 2019 Conference on Powder Metallurgy & Particulate Materials are available from the Publications Department of MPIF www.mpif.org.

**Manager Modeling, Simulation, and Fatigue, GKN Sinter Metals, Krebsöge 10, Radevormwald 42477, Germany; Email: Markus.Schneider@gknpm.com, **CAE Engineer, GKN Sinter Metals, 1670 Opdyke Court, Auburn Hills, Michigan 48326, USA*

Young's modulus, E, is less than that of fully-dense wrought steels.[1] In addition to the amount of the second phase (pore and graphite volume fraction), there is an effect of their shape. Due to the strong internal notch effect of the lamellar graphite flakes, gray cast iron variants exhibit the lowest Young's modulus. By modifying the shape of the graphite flakes, the Young's modulus can be improved. Therefore, vermicular graphite cast iron variants exhibit intermediate, and nodular cast iron variants exhibit the highest Young's modulus, respectively (for the same amount of graphite):[1,2]

$$E_l < E_v < E_n$$

In the prior equation, E_l denotes the Young's modulus of gray cast iron (lamellar graphite), E_v denotes the Young's modulus of vermicular graphite cast iron (vermicular graphite), and E_n the Young's modulus of the nodular cast iron (globular graphite) variant. A similar effect is known for PM steels. The effect of the sintered density, ρ on Young's modulus E can be described with the Balshin equation.[3] That equation describes the reduction of the pore-free density Young's modulus E_0 as function of the actual sintered density ρ. The Balshin exponent, m, is affected by the processing route and the powder used (atomized or sponge iron powder), whereas the effect of the chemical composition (alloying) is neglected:

$$E = E_0 \left(\frac{\rho}{\rho_0}\right)^m \quad (1)$$

Elevated sintering temperatures, ϑ and/or the use of sponge iron powder result in less angular pores. Therefore, the stiffness of such PM steels is a bit higher.[3] The similarity to the discussed cast iron variants is evident. The same explanation holds true for the sintered density ρ. The specific weight of the trapped gas and of the graphite flakes do not play a role compared with the high-density matrix material (iron with a full density of $\rho_0 = 7.85\ g/cm^3$). Therefore, both material classes have a certain lightweight potential. The lower load-bearing cross-section and the higher internal stress concentration due to the pores in PM steels, as well as that due to the lamellar graphite flakes in gray cast iron variants, have an impact on the static strength and ductility. In general, the material properties are inferior to fully-dense wrought steels. The other similarities are summarized in Table I.

THE SUPPORT EFFECT OF PM STEELS AND GRAY CAST IRON AND ITS DEFINITION

The observation that gray cast iron reacts more moderately to notches compared with wrought steels is very old and was derived simultaneous to the development of that material class and its fatigue testing and characterization.[4–6] Moreover, it became a design benefit for the casting industry. A similar development was achieved for sintered PM steels, whereas the investigation of notched components was always of importance.[7]

TABLE I. SIMILARITIES BETWEEN SINTERED PM STEELS AND GRAY CAST IRON

Observation/Effect	PM Steel	Gray Cast Iron	Similarity
Affected Young's modulus E	Lower stiffness due to the porosity	Lower stiffness due to the lamellar graphite flakes	Valid
Affected ultimate tensile strength σ_u and fracture strain ε_f	Lower static strength and ductility due to the porosity	Lower static strength and ductility due to the lamellar graphite flakes	Valid
Affected density ρ	Lower density (lightweight potential) due to the porosity	Lower density (lightweight potential) due to the lamellar graphite flakes	Valid
Affected fatigue notch factor K_f and support factor n_χ	The inherent pores act as internal notches and therefore the response to external geometrical notches is reduced	The inherent lamellar graphite flakes act as internal notches and therefore the response to external geometrical notches is reduced	Valid
Recommended equivalent stress definition $\sigma_{eq} = \sigma_1$	The inherent pores act as internal notches and therefore there will be a similar stress concentration effect for shear and tensile stresses respectively, resulting in similar bending and torsion fatigue strength at the knee-point values	The inherent lamellar graphite flakes act as internal notches and therefore there will be a similar stress concentration effect for shear and tensile stresses respectively, resulting in similar bending and torsion fatigue strength at the knee-point values	Valid
Affected internal friction and material damping Q^{-1}	There will be no strong internal friction mechanism solely due to the porosity	Higher internal friction due to the interface friction between the metallic matrix and the lamellar graphite flakes as well as the dislocation motion within the hexagonal structure of the graphite basal planes	Invalid
Affected thermal conductivity λ	Trapped gas will not improve the thermal conductivity	Graphite improves the thermal conductivity	Invalid

This observation is called the support effect. The support effect describes the discrepancy between the purely geometric stress concentration factor K_t and the purely empirical fatigue notch factor K_f.

For cases of simple loading and simple geometries, the stress concentration factor K_t can be estimated with tabulated handbook values.[8,9] Those tables were derived with the help of photoelastic models, with local strain gauge measurements or with analytical and numerical methods. However, for the definition of a stress concentration factor K_t a nominal stress σ_n is needed. That nominal stress σ_n can be calculated only for simple loading cases and simple geometries. Therefore, the concept is limited, and other metrics are needed to describe the stress concentration and the stress distribution in general. The fatigue notch-factor K_f is the drop in the fatigue strength at the knee-point $\sigma_A(K_t = 1)$ of a s-N line derived on unnotched fatigue samples ($K_t = 1$) compared with the fatigue strength at the knee-point $\sigma_A(K_t > 1)$ of a s-N line derived on notched fatigue samples ($K_t > 1$). It is important to note that K_f incorporates the experimental error of two experiments (error propagation law). Therefore, the derived values of the fatigue notch-factor K_f should be analyzed carefully. Moreover, due to the scatter, many experiments are needed to determine a clear tendency (cause-and-effect chain). Such a tendency could be the question of whether the fatigue notch-factor K_f is affected by the sintered density ρ, or a static strength or ductility parameter. The German FKM guideline proposes a dependency on the ultimate tensile strength σ_u. It is believed that the support effect decreases as the ultimate tensile strength σ_u increases.[10] In most cases it is found that the stress concentration factor K_t overestimates the damaging effect of notches:

$$K_t > K_f$$

There are many ways to describe or to estimate the fatigue notch factor K_f if no fatigue experimental data are available. A well-known approach in the U.S. is that from Peterson[8] and Thum:[11,12]

$$q = \left(\frac{(K_f - 1)}{(K_t - 1)} \right) \qquad (2)$$

The fatigue notch-sensitivity q is a function of the material class and the notch radius r. With its help and the known stress concentration factor K_t, the corresponding fatigue notch-factor K_f can be estimated. A perfectly notch-insensitive material exhibits a fatigue notch-sensitivity of q = 0. The opposite behavior is expected if the fatigue notch-sensitivity increases to q = 1. Several PM steels have been characterized in that manner. A good overview can be found elsewhere.[13] The problem of equation (2) is not its accuracy, it is the formulation using the stress-concentration factor K_t. Since modern fatigue life estimates are FEA simulation-based, the notch cannot be described with its stress-concentration factor K_t anymore because the definition of a nominal stress σ_n and of a nominal cross-section A fails. Therefore, another metric is needed to describe the effect of a notch on the resulting stress distribution. In general, a notch affects different characteristics of the surrounding stress distribution. Due to the reduced cross-section, the change of the stiffness and the superimposed bending moments and shear stresses, the stress distribution exhibits a strong peak stress on the part surface ("stress raiser").[14] Due to that local effect and the assumed force balance, the stress distribution becomes nonlinear and more inhomogeneous. As a result, the highly loaded material volume V_{90} is affected in a different way. This is of importance since the statistical size effect predicts an earlier failure due to the higher risk to activate crack nuclei (material inhomogeneities, pores or micro-cracks). The highly loaded material volume approach is an alternative to the support factor approach.[15] In general, it is believed that this approach is more accurate since it can predict the reduction of the fatigue strength of the knee-point σ_A of larger components with the same stress distribution. However, this approach is not supported by commercial FEA simulation-based fatigue software packages like nCode, DesignLife, or FEMFAT.[16,17]

Moreover, the stress distribution becomes multiaxial because sharp notches constrain the necking and the free deformation of the material. As a result, the stress tensor exhibits three, nonzero principal stresses σ_1, σ_2, and σ_3. The first effect ("stress raiser") can be described with the stress-concentration factor K_t. The other effects remain unclear. An alternative method to the fatigue notch-sensitivity approach of Peterson is the relative stress gradient approach from Siebel and Stieler. This approach was adopted for the German FKM guideline[10] and other guidelines, and it uses the relative stress gradient normal to the part surface χ^* as a metric for the sharpness of the stress distribution (alternative to or in addition to the definition of the stress-concentration factor K_t). The material response to that stress concentration is described with the support number n_χ (an alternative to the definition of the fatigue notch-sensitivity q) as:

$$n_\chi = \frac{K_t}{K_f} \qquad (3)$$

In a time before the FEA method found its way into stress calculations, the Peterson (fatigue notch-sensitivity q) and the Siebel and Stieler (relative stress gradient χ^*) approaches were equivalent alternatives having the same accuracy. A clear benefit of the relative stress

gradient approach arose due the implementation of the FEA method. The FEA method can support the relative stress gradient approach because the relative stress gradient χ^* can be calculated easily from the distance from node to node and the corresponding node stresses. However, several relative stress gradients can be determined on the part surface. Therefore, a proper equivalent stress σ_{eq} should be chosen. In the following, the first principal stress hypothesis (Rankine hypothesis) is used to investigate the notch effect:

$$\sigma_{eq} = \sigma_1$$

An early formulation of the support number n_χ was:

$$n_\chi = \frac{K_t}{K_f} = 1 + \sqrt{s_g \times \chi^*} \quad (4)$$

In equation (4) the only material parameter is s_g, which can be correlated with the metallurgical grain diameter d.[11,14,18] Later, the square-root dependency of the support number n_χ and the relation to the grain diameter d were replaced by Hück in a more general manner:[11]

$$n_\chi = \frac{K_t}{K_f} = 1 + a \times \chi^{*b} \quad (5)$$

In equation (5), the coefficient a and the exponent b are free parameters. There might be a limit because from the physical point of view, K_t must increase faster with an increasing relative stress gradient χ^* than its resulting support number n_χ. Otherwise, the stress-concentration factor K_t will be smaller than one. Several s-N lines with different stress-concentration factors K_t and relative stress gradients χ^* are needed for the curve fitting. The unnotched axial reference s-N line with a stress-concentration factor of $K_t = 1$ and a relative stress gradient of $\chi^* = 0$ mm^{-1} is always needed. The testing effort to derive such relations is significant. Therefore, different empirical solutions and approximations can be found in the literature as a function of the material class. Hück found the relations in Table II.

Eichlseder modified the Hück approach for the commercial FEA simulation-based fatigue software FEMFAT such that the ratio of the unnotched axial and bending fatigue strength at the knee-point $\sigma_{A,\ axial}/\sigma_{A,\ bending}$ was introduced as a reference.[17,19] Moreover, Eichlseder adopted the exponent b from Table II (Hück approach). The approach from the German FKM guideline is more complex because it incorporates the ultimate tensile strength σ_u explicit, and the support number n_χ is defined in intervals.[10] It can be written as:

$$n_\chi = 1 + \sqrt[z]{\chi^* \times 10^{-\left(a_G - y + \frac{\sigma_u}{b_G}\right)}} \quad (6)$$

In equation (6), the parameters a_G and b_G are material class dependent, whereas z and y are interval dependent (in terms of the relative stress gradient χ^*, the parameters are not listed at this position). The subsequent data analysis was done with the Hück approach because the correlation coefficient r_{xy} from the curve fitting was better than the one from the FKM guideline. Mechanical FEA simulations incorporate the stress-concentration effects automatically due to the local stress definition. This means, for comparison with an analytical nominal stress σ_n from a simple loading case (e.g., from the axial or bending fatigue testing), the nominal stress σ_n must be converted into a local stress σ:

$$\sigma = K_t \times \sigma_n \quad (7)$$

The local stress distribution from the FEA simulation can be analyzed in terms of notches by investigation of the relative stress gradient χ^*:

$$\chi^* = \left| \frac{\delta \sigma_1}{\delta s} \right|_{s=0\ mm} \times \frac{1}{\sigma_{1,max}} \quad (8)$$

The relative stress gradient χ^* describes the slope of the stress distribution $\delta\sigma_1/\delta s$ normal to the part surface. The infinitesimally small distance from the part surface (s=0 mm) is denoted by δs and can be taken from the FEA simulation. That distance can be interpreted as the distance from node to node of the FEA mesh. However, it is obvious that there is a certain mesh-size effect because the distance from node to node is finite. On the other hand, the analytical definition above exhibits the sharpest relative stress gradient χ^*. This means the solution from the FEA simulation will always underestimate the sharpness of the relative stress gradient χ^* resulting in underestimated support numbers n_χ (conservative approximation). Figure 1 shows an example of that procedure. This very accurate numerical approximation was not available when Siebel and Stieler proposed the relative stress gradient approach. They used the observation that the relative stress gradient χ^* is proportional to the notch radius r. An additional term describes the effect from the geometry, e.g., the height h of a bending specimen. A few simple loading cases are summarized in Table III.[18] Those approximations are used for the derivation of the support number diagram of the FKM guideline.

The support effect can be explained with different theories. The material behavior during the underlying

TABLE II. HÜCK PARAMETERS FOR THE SUPPORT EFFECT FOR DIFFERENT MATERIAL CLASSES[11]

Material Class	a (mm)	b (1)	σ_u (MPa)
Wrought steel (Hück)	0.450	0.300	$250 \le \sigma_u < 1{,}200$
Cast steel (Hück)	0.330	0.650	$250 \le \sigma_u < 800$
Gray cast iron (Hück)	0.430	0.680	$150 \le \sigma_u < 350$

TABLE III. APPROXIMATIONS FOR THE RELATIVE STRESS GRADIENT χ^*

Load	Geometry	χ^* (mm^{-1})
Axial	Unnotched	0
Axial	Notched	2/r
Bending	Unnotched	2/h
Bending	Notched	2/r + 2/h

FEA simulation is assumed to be linear-elastic. This simplification ignores plastic yielding, especially in notches. The stress-strain curves of sintered PM steels do not exhibit a clear elastic domain. Therefore, the yield strength, σ_y, is defined in terms of an 0.2% offset yield strength, $\sigma_{0.2}$. In reality, the linear-elastic peak stress σ will exceed that limit. The easiest way to implement the real stress-strain response into a FEA simulation-based notch analysis is to apply the Neuber hyperbola on the linear-elastic peak stress as shown in Figure 2. In this case a peak stress of 1,217.5 MPa could be reduced to 737 MPa (for FLDN4C2-4905 with a sintered density of ρ = 7.0 g/cm^3). Neuber had introduced the concept of the macro (static loading) and micro (cyclic loading) support effect, respectively.[9] With this approach, the local yielding and the stress rearrangement can be predicted quite accurately. The contribution of that effect on the support number n_χ is denoted with n_{Neuber}.

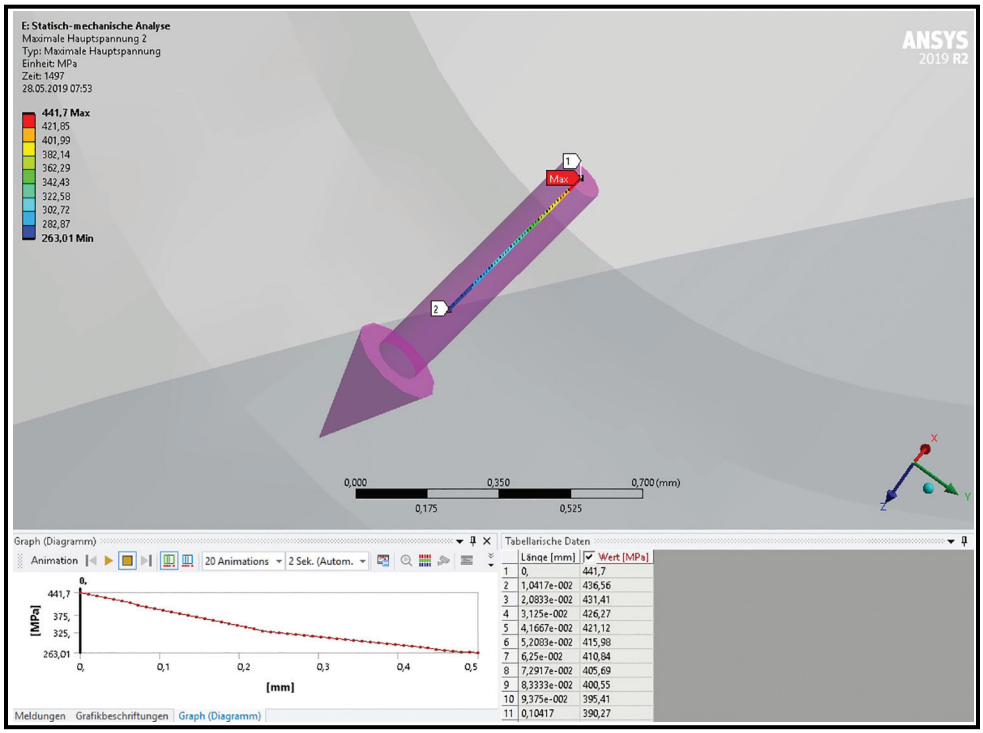

Figure 1. *Estimation of the relative stress gradient χ^* from a linear-elastic stress FEA simulation*

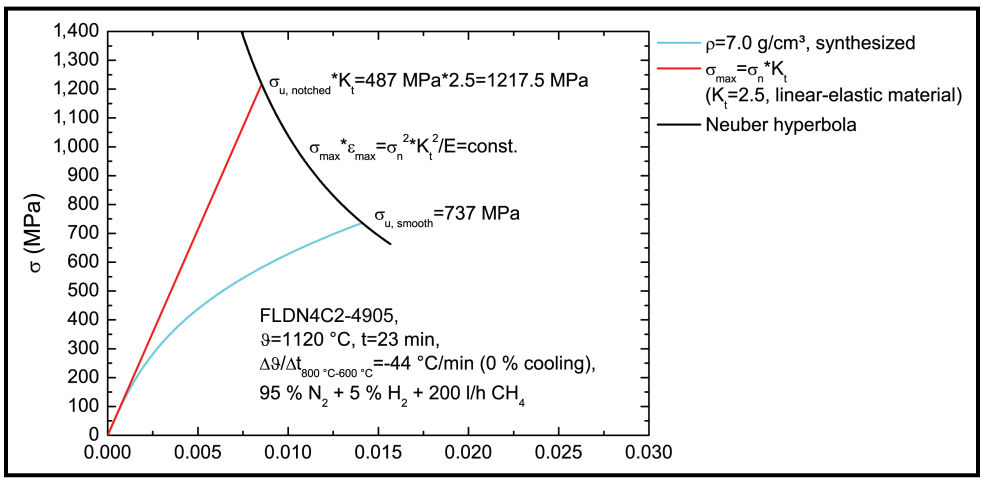

Figure 2. *Notch-root analysis with the Neuber hyperbola (macro support effect, static loading)*

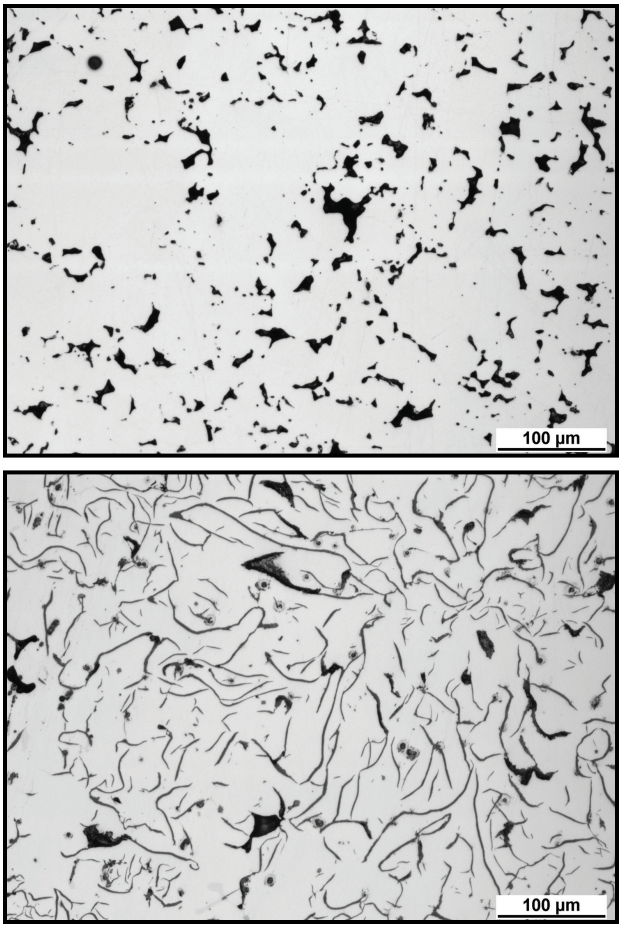

Figure 3. *Defect population (porosity) of a sintered PM steel (for FD-0205 with a sintered density of ρ = 7.2 g/cm³), (top) and defect population (lamellar graphite flakes) of a gray cast iron variant (here GG 25~ASTM A48 with a cast density of ρ = 7.14 g/cm³), (bottom)*

Another contribution could come from the different crack propagation rates da/dN in the Paris regime (da/dN-ΔK curves) from notched and unnotched specimens, respectively.[12] Depending on the surrounding stress field, the total fatigue lifetime N can be decomposed into the crack initiation phase $N_{crack\ initiation}$ and the crack propagation phase $N_{crack\ propagation}$, respectively:[10,12,20]

$$N = N_{crack\ initiation} + N_{crack\ propagation}$$

The result in terms of the support number n_χ is called n_{Paris} and it describes the deceleration of the crack propagation rate da/dN in an inhomogeneous stress field. However, that contribution does not play a role until a crack is present (crack propagation phase). Another important contribution is based on statistical considerations, as briefly discussed above with the highly loaded-material volume V_{90}. The weakest-link theory results in the Weibull distribution. That probability distribution can be used to link the highly-loaded-material volume V_{90} (or any other definition) to a certain survival probability level P_s. In other words, the risk of failure increases with an increasing material volume V. Generally, the low notch-sensitivity of cast iron variants is explained with its inherent defect population. The graphite flakes act as internal notches and therefore the response to external geometrical notches is reduced.[21] A similar explanation can be used for the porosity of sintered PM steels. The inherent pores act as internal notches and therefore the response to external geometrical notches is reduced. That old observation can be explained with the Weibull distribution.[4,5,6,21] Its contribution to the support number n_χ is called $n_{Weibull}$. Figure 3 compares the microstructures of both material classes. The similarity of both material classes is evident. However, the grain-size distributions are not visible because the microstructures have not been etched. Moreover, the fine lamellar graphite flakes of the GG 25

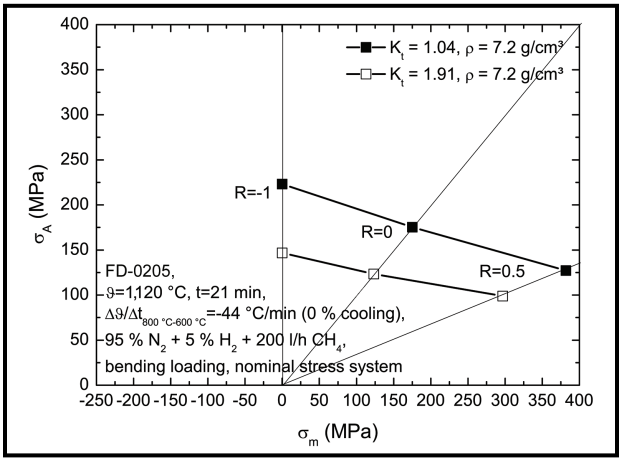

Figure 4. *Haigh diagram of FD-0205 with a sintered density of ρ = 7.2 g/cm³ in the unnotched (bending loading mode, K_t = 1.04 ≈ 1) and the notch condition (bending loading mode, K_t = 1.91)*

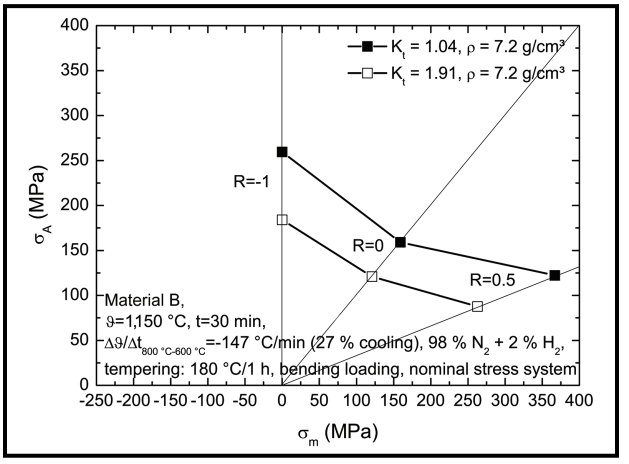

Figure 5. *Haigh diagram of Material B with a sintered density of ρ = 7.2 g/cm³ in the unnotched (bending loading mode, K_t = 1.04 ≈ 1) and the notch condition (bending loading mode, K_t = 1.91)*

gray cast iron variant appear much sharper. These microstructural details (grain diameter d, and the internal notch-effect) could explain the different support numbers n_χ shown later in Table V and in Figure 6.

The defined support factor n_χ can be decomposed into its three components as:[10,20]

$$n_\chi = n_{Neuber} \times n_{Paris} \times n_{Weibull} \quad (9)$$

From this equation it can be seen that three different phenomena have an influence on material notch-sensitivity. The plasticity, the microstructure, and the defect population have a major effect.

RESULTS

The support effect was investigated in detail because an understanding of the behavior of notched components is essential for the PM industry. Moreover, the low notch-sensitivity is a benefit for complex-shaped components due to near-net-shape design capabilities. In general, a sintered PM material is characterized with 12 s-N lines at GKN Sinter Metals Engineering GmbH. Three loading ratios R (R = -1, R = 0, and R = 0.5) are used for each sintered density ρ (where $R = \sigma_{min}/\sigma_{max}$). With those three loading ratios, R, the whole right-hand side (with tensile mean stresses σ_m) of the Haigh diagram and the resulting Haigh damage line can be characterized as shown for FD-0205 with a sintered density of ρ = 7.2 g/cm^3 in Figure 4 and for Material B (Ancorsteel 4300 + 0.6 wt.% gr. + 0.25 wt.% MnS) with a sintered density of ρ = 7.2 g/cm^3 in Figure 5. The sintered density ρ is varied on three levels (in most cases: ρ = 6.8 g/cm^3, ρ = 7.0 g/cm^3, and ρ = 7.2 g/cm^3) to achieve the property-density correlation (Balshin approach). The fatigue specimens used are unnotched and correspond to DIN EN ISO 3928. The result of the s-N line is the fatigue strength at the knee-point $\sigma_A(K_t \approx 1)$. Modern FEA simulations have shown that there is a negligibly small stress concentration (K_t = 1.04 ≈1). The loading mode is always flat bending because that loading mode is very robust and tolerant against shape deviations. Moreover, in contrast to the axial loading mode, the bending loading mode is not sensitive to superimposed bending moments. Furthermore, a turning operation (as for rotation bending), which densifies the microstructure is not needed (superimposed effects from residual stresses σ_R, strain hardening, densification, and surface roughness). The remaining three s-N lines are recorded for notched fatigue specimens with a notch radius of r = 0.9 mm according DIN EN ISO 3928. The resulting stress-concentration factor K_t for the bending loading mode is K_t = 1.91 (slightly higher than the proposed stress-concentration factor K_t in the standard). The result of the s-N line is the fatigue strength at the knee-point $\sigma_A(K_t = 1.91)$. Therefore, the fatigue notch-factor K_f is based on the stress-concentration factor K_t = 1.91. In that case the loading ratio is R = -1. Therefore, it is assumed that the Haigh damage line can be shifted in parallel without changing the mean stress sensitivities M_1, M_2, M_3, and M_4.

A problem arises from the bending loading mode regarding the definition of a proper reference relative stress gradient χ*. The unnotched axial reference s-N line with a stress-concentration factor of K_t = 1 is always needed as reference because the relative stress gradient is χ* = 0 mm^{-1} (Table III). This problem is solved because the correlation between unnotched bending and axial s-N lines is well-documented in the literature.[22] Even if the ratio between the bending fatigue strength at the knee-point $\sigma_{A,\,bending}$ and the axial fatigue strength at the knee-point $\sigma_{A,\,axial}$ (for both values: R = -1 and K_t ≈1) shows a slight material dependency, a very good estimate is:

$$\frac{\sigma_{A,axial}}{\sigma_{A,bending}} \approx 0.85$$

With this assumption, three data pairs are available for the Hück approach (Eichlseder introduced that finding in a similar way) and the support number n_χ curve fitting. If the unnotched fatigue specimens according DIN EN ISO 3928 are tested in the upright position, the relative stress gradient for bending is simply χ* = 2/h = 2/5 mm = 0.4 mm^{-1} (Table III). The relative stress gradient for the notched DIN EN ISO 3928 specimen (r = 0.9 mm, K_t = 1.91) for the bending loading mode is χ* = 2/r + 2/h = 2/0.9 mm + 2/5 mm = 2.622 mm^{-1} (Table III). A subsequently performed FEA simulation came to a slightly different result with χ* = 2.524 mm^{-1}. The results for a wide range of different sintered PM steels and densities ρ are summarized in terms of the Hück approach in Table IV. It can be seen that the Hück coefficients vary between a = 0.226 mm to a = 0.405 mm, whereas the Hück exponents vary between b = 0.268 to b = 1.010. These values are extreme cases and they do not represent the typically achievable support effect. Therefore, the mean values, a = 0.329 mm and b = 0.736, are more representative (average of all 21 in-house data sets, the three data sets from the literature survey, and the data set from Table VII). Based on the huge experimental effort, these parameters can be assumed typical for sintered PM steels. Therefore, Table II can be expanded with the material class of sintered PM steels as shown in Table VI. The high Hück exponent b of sintered PM steels shown in Table VI leads to the conclusion that sintered PM steels are superior to most of the other material classes, especially for very sharp notches (high relative stress gradient χ*). However, gray cast iron with its high Hück coefficient of a =

TABLE IV. HÜCK PARAMETERS FOR SINTERED PM STEELS
(21 in-house data sets and three data sets from the literature survey), derived on s-N lines recorded with a loading ratio of R=-1

Material	ρ (g/cm³)	σ_A (K_t=1) (MPa)	σ_A (K_t=1.91) (MPa)	K_f (1)	σ_u (MPa)	a (mm)	b (1)
Material A	6.70	187.88	145.72	1.29	551	0.361	0.780
Material A	6.90	217.28	164.61	1.32	597	0.351	0.750
Material A	7.00	240.58	166.54	1.44	624	0.312	0.622
Material B, HTS, rapid cooled + tempered	6.80	200.42	154.77	1.29	752	0.359	0.775
Material B, HTS, rapid cooled + tempered	7.00	222.37	177.93	1.25	857	0.374	0.819
Material B, HTS, rapid cooled + tempered	7.20	259.47	183.95	1.41	982	0.322	0.658
Material C, rapid cooled + tempered	6.80	210.82	165.27	1.28	901	0.365	0.794
Material C, rapid cooled + tempered	7.00	245.89	182.62	1.35	1,022	0.342	0.723
Material C, rapid cooled + tempered	7.20	278.81	228.13	1.22	1,177	0.383	0.846
Material C	6.80	169.51	127.95	1.32	690	0.350	0.748
Material C	7.00	186.35	160.58	1.16	796	0.405	0.906
Material C	7.20	244.00	184.58	1.32	853	0.350	0.748
FD-0205	6.80	171.45	122.96	1.39	526	0.327	0.675
FD-0205	7.00	196.42	133.50	1.47	585	0.304	0.594
FD-0205	7.20	223.21	146.65	1.52	670	0.289	0.539
FLDN4C2-4905	6.80	220.50	126.50	1.74	650	0.226	0.268
FLDN4C2-4905	7.00	245.65	173.44	1.42	724	0.321	0.652
FLDN4C2-4905	7.20	288.36	198.96	1.45	849	0.311	0.617
FC-0205	6.80	151.78	108.30	1.40	430	0.325	0.667
FC-0205	7.00	172.50	128.12	1.35	488	0.342	0.723
FC-0205	7.20	178.35	141.93	1.26	541	0.372	0.812
FD-0405	7.00	Literature survey, based on differently notched specimens				0.306	0.857
Material D	7.00	Literature survey, based on differently notched specimens				0.282	0.986
FC-0205**	7.00	Literature survey, based on differently notched specimens				0.258	1.010

Material A = Iron + 3 wt.% Cu + 0.55 wt.% P + 0.55 wt.% graphite
Material B = Ancorsteel 4300 + 0.6 wt.% graphite + 0.25 wt.% MnS (Ancorsteel 4300 = 1.0 wt.% Cr, 1.0 wt.% Ni, 0.8 wt.% Mo, 0.6 wt.% Si, 0.1 wt.% Mn); HTS = high temperature sintered
Material C = Distaloy DH-1 + 0.65 wt.% graphite (Distaloy DH-1 = FL-4900 with 2 wt.% Cu diffusion alloyed)
Material D = Atomet4901 + 2 wt.% Cu + 0.65 wt.% graphite
FD-0205 contained 0.5 wt.% graphite
FD-0405 contained 0.6 wt.% graphite
FC-0205 = Ancorsteel 1000B Mn + 2 wt.% Cu + 0.6 wt.% graphite
FC-0205** = Ancorsteel 1000B Mn + 1.5 wt.% Cu + 0.6 wt.% graphite

0.430 mm seems to be slightly better (Figure 6).

This observation provokes the question of the effect of the metallurgical grain diameter d on the support effect. Note that the Hück coefficient, a, replaced the material parameter, s_g, in the equations presented. The corresponding ultimate tensile strength σ_u was recorded for every in-house data set. According the Balshin equation, the progressive increase of the ultimate tensile strength σ_u with an increasing sintered density ρ can be seen directly in Table IV. In contrast to the FKM guide-

line prediction there is no trend regarding the ultimate tensile strength σ_u. Even hard materials with a high ultimate tensile strength σ_u and a low ductility show a strong support effect. From the current data sets there is neither a clear correlation between the ultimate tensile strength, σ_u, and the Hück coefficient, a, nor between the Hück exponent, b. This is a fantastic finding since the FKM guideline assumes a reduction of the support number, n_χ for high strength materials as shown in Table V. Only two materials show the expected tendency. The notch-fatigue factors, K_f, increase for Material A (Iron + 3 wt.% Cu + 0.55 wt.% P + 0.55 wt.% gr.) and for FD-0205 as a function of the ultimate tensile strength, σ_u, and over the Balshin equation as a function of the density, ρ, respectively. However, extraordinary hard materials (quenched with faster quenching agents than gas) were not tested yet. Whether hardened PM steels exhibit potentially lower support numbers n_χ must be investigated in the future n_χ. However, the homogeneity of the microstructure from sintered prealloyed powders could play a role as investigated by Ericson, and should be studied further.[13] Since the ultimate tensile strength, σ_u, of sintered PM steels (within a special alloying system) is a function of the sintered density, ρ, the expected density effect (Weibull) cannot be extracted (Figure 7 and Figure

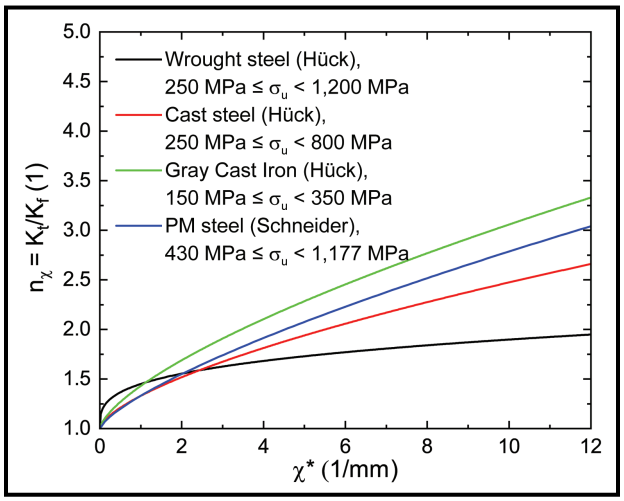

Figure 6. *Support number diagram based on the parameters given in Table VI*

TABLE V. EFFECT OF THE ULTIMATE TENSILE STRENGTH, σ_u, ON THE SUPPORT NUMBER n_χ FOR A RELATIVE STRESS GRADIENT OF $\chi^* = 2.524\ mm^{-1}$. THE FKM GUIDELINE PREDICTS A DROP OF THE SUPPORT NUMBER n_χ FOR HIGH STRENGTH MATERIALS, WHEREAS THAT TENDENCY CANNOT BE RECOGNIZED FROM THE CURRENT DATA SETS FOR SINTERED PM STEELS (HÜCK APPROACH, INDEPENDENT OF THE ULTIMATE TENSILE STRENGTH, σ_u)

σ_u (MPa)	n_χ (1) for the material class of gray cast iron according the FKM guideline (parameters: z = 4, y = 0, a_G = -0.05, and b_G = 3,200 MPa)	n_χ (1) for the material class of sintered PM steel according that study (Hück approach)
430	2.04	1.65
500	1.99	1.65
600	1.92	1.65
700	1.85	1.65
800	1.80	1.65
900	1.74	1.65
1,000	1.69	1.65
1,100	1.64	1.65
1,177	1.61	1.65

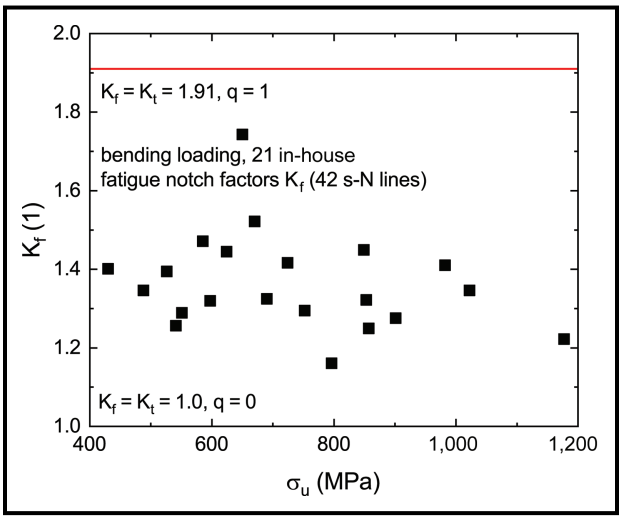

Figure 7. *Fatigue notch-factors, K_f, as function of the ultimate tensile strength, σ_u. An increase of the fatigue notch factor K_f (decrease of the support number n_χ) cannot be recognized for the sintered PM steels investigated*

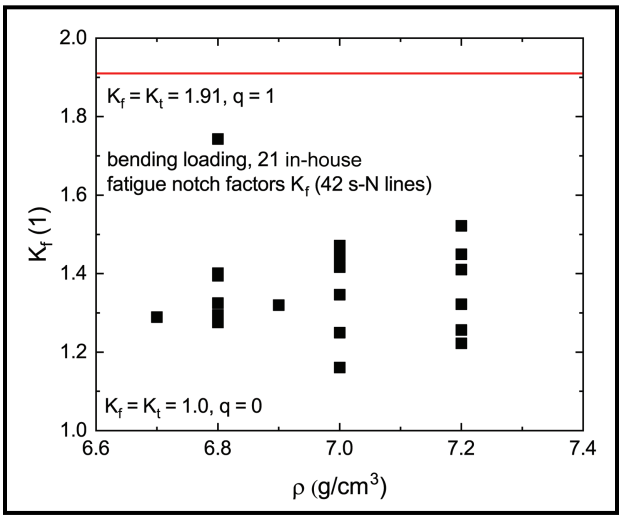

Figure 8. *Fatigue notch-factors, K_f, as function of the sintered density, ρ. An increase of the fatigue notch factor, K_f, (decrease of the support number n_χ) cannot be recognized for the sintered PM steels investigated*

TABLE VI. HÜCK PARAMETERS FOR THE SUPPORT EFFECT FOR DIFFERENT MATERIAL CLASSES.[11] THE ADDITIONAL MATERIAL CLASS OF SINTERED PM STEELS IS A RESULT OF THIS STUDY

Material Class	a (mm)	b (1)	σ_u (MPa)
Wrought steel (Hück)	0.450	0.300	$250 \leq \sigma_u < 1{,}200$
Cast steel (Hück)	0.330	0.650	$250 \leq \sigma_u < 800$
Gray cast iron (Hück)	0.430	0.680	$150 \leq \sigma_u < 350$
PM steel (Schneider)	0.329	0.736	$430 \leq \sigma_u < 1{,}177$

TABLE VII. HÜCK PARAMETERS FOR SINTERED PM STEELS[19]

Material Class	a (mm)	b (1)	σ_u (MPa)
PM steel (Götz)	0.300	0.830	Not defined

TABLE VIII. NOTCH-FATIGUE FACTORS K_f AS FUNCTION OF THE LOADING RATIO, R, FROM FIGURE 4 AND FIGURE 5

Material	R (1)	σ_A (K_t = 1) (MPa)	σ_A (K_t = 1.91) (MPa)	K_f (1)
FD-0205, ρ = 7.2 g/cm^3	-1	223.21	146.65	1.52
FD-0205, ρ = 7.2 g/cm^3	0	175.22	123.27	1.42
FD-0205, ρ = 7.2 g/cm^3	0.5	127.27	98.95	1.29
Material B, ρ = 7.2 g/cm^3	-1	259.47	183.95	1.41
Material B, ρ = 7.2 g/cm^3	0	159.20	120.81	1.32
Material B, ρ = 7.2 g/cm^3	0.5	122.28	87.58	1.40

8). However, the recorded ultimate tensile strength values vary between σ_u = 430 MPa to σ_u = 1,177 MPa. Therefore, the support effect from the material class of sintered PM steels (Table VI) can be described in a similar way to Table II. The resulting in-house data set for that material class is given in Table VI.

Table V provides an overview of the predicted reduction of the support number, n_χ for the material class of gray cast iron (parameters: z = 4, y = 0, a_G = -0.05, and b_G = 3,200 MPa) according the FKM guideline for a range of ultimate tensile strength between σ_u = 430 MPa to σ_u = 1,177 MPa. This range was chosen because of the in-house data sets from Table IV. The corresponding relative stress gradient was kept constant with χ^* = 2.524 mm^{-1} because that value represents the notched DIN EN ISO 3928 specimen (r = 0.9 mm, K_t = 1.91) for the bending loading mode.

Figure 7 summarizes the in-house fatigue notch-factors, K_f, from Table IV. For the derivation of the 21 in-house data sets, the recording of 42 s-N lines was needed. The overall variants averaged fatigue notch factor is K_f = 1.36 (for K_t = 1.91) resulting in an average fatigue notch sensitivity of q = 0.40.

The scatter-band in Figure 8 is too large to derive some conclusions. There might be some outliers, but the identification of a few outliers from a population of n = 21 data sets is hardly possible. Nevertheless, the clustering of the 21 in-house data sets seems to be a bit more systematic than the scatter-cloud from Figure 7.

The 21 in-house data sets, the three data sets from the literature survey, and the data set from Table VII are averaged regarding the Hück coefficient a and the Hück exponent, b. Table VI exhibits the Hück parameters for four different material classes. With those numbers the local stress, σ from a linear elastic FEA simulation can be corrected to match the experimental results and to figure out the advantage of sintered PM steels. The only parameter needed is the relative stress gradient, χ^*, which can be estimated from the distance from node to node and the corresponding node stresses from the linear-elastic FEA simulation or with the help from Table III. From Table VIII, Figure 4, and from Figure 5 it can be concluded that each stress component from the linear-elastic FEA simulation, the cyclic stress amplitude σ_A and the static mean stress σ_m, must be corrected to achieve a parallel shifting of the Haigh damage line without changing the mean stress sensitivities M_1, M_2, M_3, and M_4. The parallel shifting of the Haigh damage line will be conservative with a support number, n_χ derived with a loading ratio of R = -1. Soft and ductile materials such as FD-0205 with a sintered density of ρ = 7.2 g/cm^3 (Figure 4) show a further decreasing of the notch-sensitivity with an increasing mean stress σ_m. That is due to a more pronounced plastic yielding and a higher contribution of n_{Neuber}. The shifting of the Haigh damage line in the mean stress, σ_m, direction is due to the macro support effect (static loading) solely. This means sintered PM steels are also notch insensitive during static loading (stress-strain curve).

The opposite behavior is expected for hard and less ductile materials such as Material B with a sintered density of ρ = 7.2 g/cm^3 (Figure 5). The assumption of a parallel shifting of the Haigh damage line seems to be more correct in this case. There is no pronounced plastic yielding for higher loading ratios, R.

Götz proposed a similar data set for sintered PM steels based on published fatigue experiments (Table VII).[19]

The effect of the loading ratio, R, on the notch-fatigue factor K_f can be taken from Table VIII. As mentioned before, the soft and ductile FD-0205 material, with a sintered density of ρ = 7.2 g/cm^3, exhibits decreasing notch-fatigue factors K_f with an increasing loading ratio, R, whereas the hard and less ductile Material B, with a sintered density of ρ = 7.2 g/cm^3, shows more or less constant notch-fatigue factors K_f.

CONCLUSIONS

The support effect of sintered PM steels is discussed. The support effect is much more than a detail in mate-

rials science. It is one reason why sintered PM steels can compete mechanically with wrought steels. Wrought steels are tougher and they exhibit much higher values of fatigue strength at the knee-point, σ_A, in the unnotched condition. However, there are few mechanical engineering components without functional geometrical elements, e.g., holes, shoulder fillets, teeth, protuberances, changing cross-sections, and keyways. All these geometric elements affect the resulting stress distribution. Therefore, the unnotched s-N line has only a limited explanatory power. A comparison between wrought steels and sintered PM steels in the notched condition can reverse this ranking. Moreover, sintered PM steels and components are distinguished from other manufacturing techniques due to their near-net-shape design capabilities. Even if the reduction of the "stress raisers" through product design is the best approach to increase the fatigue lifetime N of that component, in many cases that approach is not applicable for functional reasons (geometrical elements cannot be changed, the customer is responsible for the design, and ignorance of fatigue considerations in a design proposal). It is fortunate that a material class exhibits this combination of a high degree of design freedom/near-net-shape design capabilities and a low notch sensitivity.

The derived Hück parameters for sintered PM steels (a = 0.329 mm and b = 0.736) are recommended to implement the support effect into the FEA simulation-based fatigue lifetime predictions. It should be pointed out that the porosity plays an ambivalent role here. On the one hand it reduces the smooth, unnotched strength properties. On the other hand, the porosity is one reason for the low notch-sensitivity and the higher local fatigue strength in the notched condition. Twenty-one in-house data sets confirm this observation. The benefits of sintered PM steels have three dimensions.

- Near-net-shape design capabilities with good tolerances for a primary shaping manufacturing method
- Cost-efficient solution for the mass production of parts
- High local fatigue strength due to the very high support effect

The relative stress gradient approach described and the corresponding support number, n_χ can be applied easily in practice resulting in more business wins and a much better agreement between the FEA simulation-based fatigue lifetime predictions and the observations from the testing field. Note that the bending fatigue strength at the knee-point σ_A values must be corrected (e.g., from Figure 4 and Figure 5) with the factor of 0.85 for a correct application of the support number, n_χ. This is because those bending values exhibit a relative stress gradient of $\chi^* \neq 0$ mm^{-1}. Moreover, that approach is the backbone of modern commercial FEA simulation-based fatigue software. However, it was never the goal of the PM powder producers and the PM part makers to develop a powder with a microstructure, pore-size distribution, pore-shape distribution, and grain-size distribution tailored for a high support effect. This could be a scientific topic for the future. The role of the homogeneity of the microstructure from sintered prealloyed powders should be investigated in more detail. Moreover, the effect of less irregular pores (potentially lower internal notch effect) from high temperature sintering (HTS) and the effect of the grain size (grain diameter d) on the support effect are of interest. A correlation between the support effect and the density, ρ, is still missing. Therefore, the minimum quantity of porosity leading to a significant support effect cannot be estimated. More data sets are needed to extract a potential trend from the scatter cloud. The results from Table VI are summarized graphically in the support factor diagram in Figure 6.

REFERENCES

1. L.-Y. Fang, K. E. Metzloff, R. C. Voigt and C. R. Loper Jr., "Young's Modulus in Graphitic Cast Irons", Proc. 61st World Foundry Congress, International Academic Publishers, Beijing, China, 1995, pp. 417–428.
2. G. Pusch, P. Trubitz and B. Rehmer, "Bestimmung der elastischen Konstanten von Gußeisenwerkstoffen", Konstruieren und Gießen, 2001, vol. 26, no. 3, pp. 4–15.
3. C. Sander and P. Beiss, "Elastische Eigenschaften von Sintereisen- und stahl", IWM/RWTH Aachen, Germany, pp. 113–119.
4. O. Graf, *Die Dauerfestigkeit der Werkstoffe und der Konstruktionselemente,* First Edition, 1929, Springer Verlag, Berlin, Germany.
5. W. Herold, *Die Wechselfestigkeit Metallischer Werkstoffe,* First Edition, 1934, Springer Verlag, Wien, Austria.
6. A. Thum, "Gestaltfestigkeit und Konstruktion", Lilienthal-Gesellschaft für Luftfahrtforschung Jahrbuch 1936, pp. 75–93.
7. G. Zapf and J. Niessen, *Untersuchung des Einflusses verschiedener Vorspannungen auf die Dauerfestigkeit von Sinterwerkstoffen,* First Edition, 1973, Westdeutscher Verlag, Opladen, Germany.
8. R. E. Peterson, *Stress Concentration Factors,* First Edition, 1974, John Wiley & Sons, New York, NY.
9. H. Neuber, *Kerbspannungslehre,* Fourth edition, 1985, Springer Verlag, Berlin, Germany.
10. B. Hänel, E. Haibach, T. Seeger, G. Wirthgen and H. Zenner, *Rechnerischer Festigkeitsnachweis Für Maschinenbauteile,* Sixth Edition, 2012, VDMA Verlag, Germany.
11. D. Radaj and M. Vormwald, *Ermüdungsfestigkeit,* Third Edition, 2007, Springer Verlag, Berlin, Germany.
12. N. E. Dowling, *Mechanical Behavior of Materials,* Fourth Edition, 2012, Pearson Education Limited, New York, NY.
13. H. Ericson, "Influencers of Notches on Fatigue Behavior of PM Steels", 2003, Master's Thesis, Lulea University of Technology.
14. J. Schijve, *Fatigue of Structures and Materials,* Second Edition, 2009, Springer Verlag, Berlin, Germany.
15. A. Zafari, K. Lipp and P. Beiss, "Einfluss äußerer Kerben auf die Schwingfestigkeit von Sinterstahl", 2010, AVIF A 253, IWM/RWTH Aachen, LBF, Aachen, Germany.
16. Team of authors, *DesignLife Theory Manual,* 2013, HBM, Southfield, MI.
17. Team of authors, *FEMFAT SeminarNotes,* 2013, Magna Powertrain, St. Valentin, Austria.
18. M. Klesnil and P. Lukas, *Fatigue of Metallic Materials,* Second Edition, 1992, Elsevier, New York, NY.
19. S. Götz, "Weiterentwicklung eines bruchmechanischen Konzepts zur formzahlfreien Abschätzung der Dauerfestigkeit gekerbter Strukturen am Beispiel verschiedener Sinterstähle", 2012, Dr.-Ing. Dissertation, TU Dresden, Germany.
20. M. Wächter, C. Müller and A. Esderts, *Angewandter Festigkeitsnachweis nach der FKM-Richtlinie,* First Edition, 2017, Springer Vieweg, Wiesbaden, Germany.
21. E. Piwowarsky, *Gußeisen,* Second Edition, 1951, Springer Verlag, Berlin, Germany.
22. P. Beiss, "Stress Controlled Fatigue Testing of Porous Sintered Steels—An Endless Task", *Advances in Powder Metallurgy & Particulate Materials—2008,* compiled by R. Lawcock, A. Lawley, FAPMI, and P.J. McGeehan, Metal Powder Industries Federation, Princeton, NJ, 2008, vol. 4, part 11, pp. 60–83. ijpm